



Since January 2020 Elsevier has created a COVID-19 resource centre with free information in English and Mandarin on the novel coronavirus COVID-19. The COVID-19 resource centre is hosted on Elsevier Connect, the company's public news and information website.

Elsevier hereby grants permission to make all its COVID-19-related research that is available on the COVID-19 resource centre - including this research content - immediately available in PubMed Central and other publicly funded repositories, such as the WHO COVID database with rights for unrestricted research re-use and analyses in any form or by any means with acknowledgement of the original source. These permissions are granted for free by Elsevier for as long as the COVID-19 resource centre remains active.



# Automated screening of COVID-19 using two-dimensional variational mode decomposition and locally linear embedding

Liyuan Ma <sup>a,b</sup>, Xipeng Xu <sup>a,b</sup>, Changcai Cui <sup>a,b,\*</sup>, Jingyi Lu <sup>c,d</sup>, Qifeng Hua <sup>e</sup>, Hao Sun <sup>f</sup>

<sup>a</sup> National and Local Joint Engineering Research Center for Intelligent Manufacturing Technology of Brittle Material Products, Huaqiao University, Xiamen 361021, China

<sup>b</sup> Institute of Manufacturing Engineering, Huaqiao University, Xiamen 361021, China

<sup>c</sup> School of Electrical and Information Engineering, Northeast Petroleum University, Daqing 163318, China

<sup>d</sup> Heilongjiang Provincial Key Laboratory of Networking and Intelligent Control, Northeast Petroleum University, Daqing 163318, China

<sup>e</sup> Department of Radiology, Hwa Mei Hospital, University of Chinese Academy of Sciences, Ningbo, 315010, China

<sup>f</sup> School of Mechanical Engineering, Fuzhou University, Fuzhou, 350108, China

## ARTICLE INFO

### Keywords:

Two-dimensional variational mode decomposition  
Locally linear embedding  
Gabor filter  
Particle swarm optimization  
Support vector machine

## ABSTRACT

In order to aid imaging physicians to effectively screen chest radiography medical images for presence of Coronavirus Disease 2019 (COVID-19), a novel computer aided diagnosis technology for automatic processing of COVID-19 images is proposed based on two-dimensional variational mode decomposition (2D-VMD) and locally linear embedding (LLE). 2D-VMD algorithm is used to decompose normal and COVID-19 images, and then feature extraction of intrinsic mode functions (IMFs) using Gabor filter. To better extract low-dimensional parameters which are useful for COVID-19 diagnosis, the performance of two dimensionality reduction techniques of principal component analysis (PCA) and LLE are compared, and the LLE is shown to offer satisfactory effect of dimension reduction. Thereafter, the particle swarm optimization-support vector machine (PSO-SVM) algorithm is used to classify. The simulation results show that the proposed technology has achieved accuracy of 99.33%, precision of 100%, recall of 98.63% and F-Measure of 99.31%. Hence, the developed diagnosis technology can be used as an important auxiliary tool to assist diagnosis of imaging physicians.

## 1. Introduction

The year 2019 saw outbreak of Coronavirus Disease 2019 (COVID-19), the acute respiratory infectious disease caused by a virus that attacks lungs (among other organs). It is reported that the number of confirmed COVID-19 cases has exceeded 250 million all over the world by November 2021. The outbreak of COVID-19 not only has brought huge threat to life in many countries and regions, but also has seriously hindered development of the world economy [1–4]. Control of the epidemics is hugely dependent on early diagnosis, timely isolation and treatment.

In clinical practice, medical imaging technologies such as chest radiography (chest X-ray) [1,5], magnetic resonance imaging (MRI) [6, 7] and computed tomography (CT) [8] can provide tremendous help in screening of COVID-19. In clinics, most of the chest X-ray images of the COVID-19 patients are abnormal. Therefore, it is necessary to employ imaging techniques as an important auxiliary tool in COVID-19 screening. However, the application of imaging techniques is hampered

by shortage of physicians and advanced methods for image analysis. Furthermore, if patient's condition changes rapidly in a short period, it would bring severe challenges for imaging physicians to make diagnoses based on multiple images. Therefore, developing computer-aided diagnosis (CAD) technology would help physicians make judgments through automatic detection and screening, and thus improve diagnosis efficiency and accuracy [9].

It is worth mentioning that excellent performance of CAD in the screening of medical images has received great attention in research community. Both discrete wavelet transform (DWT) and principal component analysis (PCA) have been applied to obtain optimized feature vectors, and then feed-forward back propagation artificial neural network (ANN) and k-nearest neighbor (k-NN) have been utilized for classification of MRI [10]. A classification algorithm has been designed using a combination of DWT and support vector machine (SVM) [6]. In order to improve the accuracy of classification, stationary wavelet

\* Corresponding author at: National and Local Joint Engineering Research Center for Intelligent Manufacturing Technology of Brittle Material Products, Huaqiao University, Xiamen 361021, China.

E-mail address: [cuichc@hqu.edu.cn](mailto:cuichc@hqu.edu.cn) (C. Cui).

<https://doi.org/10.1016/j.bspc.2022.103889>

Received 28 March 2022; Received in revised form 19 May 2022; Accepted 12 June 2022

Available online 22 June 2022

1746-8094/© 2022 Elsevier Ltd. All rights reserved.

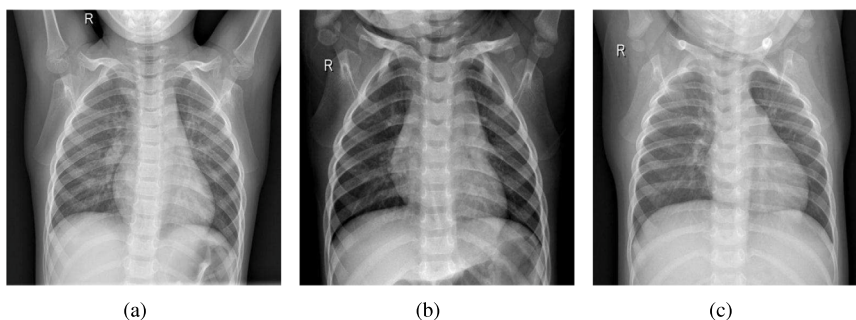


Fig. 1. Examples of the normal images.

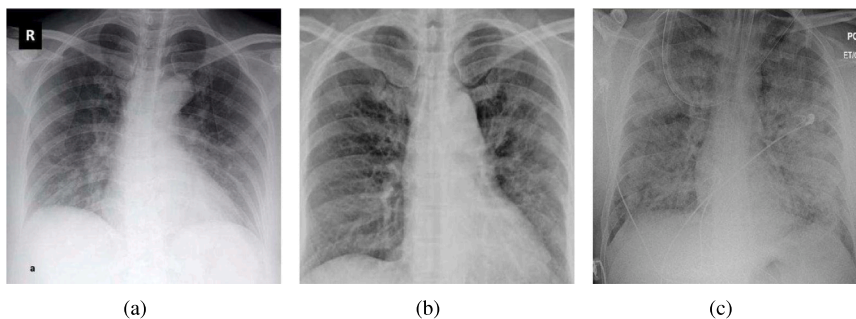


Fig. 2. Examples of the COVID-19 images.

transform (SWT) has been used in combination with PCA to get sensitive characteristic vectors, which then used as input into SVM [11]. Autoregressive (AR) Burg method has been employed in extracting feature vectors and different classifiers (e.g., k-NN, SVM and decision tree) have been used to test the accuracy of classification [12]. Two-dimensional discrete wavelet transform (2D-DWT) has been utilized in feature extraction of MRI, then both PCA and linear discriminate analysis (LDA) have been utilized to reduce feature dimension, and subsequently classification is implemented via SVM and k-NN [13]. A classification algorithm has been designed using kernel principal component analysis (KPCA) and SVM, and it is used to distinguish two classes of medical images [14].

In view of this, an automatic diagnosis technology of medical image has been recently paid some initial attention based on a combination of SVM and two-dimensional variational mode decomposition (2D-VMD) [15,16]. The 2D-VMD method was developed based on the variational mode decomposition (VMD) [17], which has been widely used in the field of image processing. Many scholars have managed to combine 2D-VMD method with SVM in the diagnosis of pathological images. The 2D-VMD method has been used to decompose MRI images, and then SVM has been used for classification with accuracy of 90.68%, sensitivity of 99.43% and specificity of 87.95% [18]. Both 2D-VMD method and least squares support vector machine (LS-SVM) have been employed to achieve automated detection of glaucoma, and have achieved better classification effect [19]. The 2D-VMD method has been used to decompose images, and SVM has been employed to automated screening of congestive heart failure [20].

Condition of COVID-19 patients can change rapidly, and as the result, it would bring the need to interpret a large number of images resulting in a heavy workload for imaging physicians. At the same time, more accurate methods to interpret images of COVID-19 patients are needed to reduce the incidence of misdiagnosis. To accomplish these tasks, one would need to address the following questions. First, how to better extract features from an image? Second, how to reduce redundant features of same performance or similarity? And third, how to automatically diagnose COVID-19 images in a more accurate way? Motivated by the above challenges, in this paper, we propose an automatic

screening method to detect COVID-19. The main contributions of the paper can be summarized as: (1) LLE algorithm is employed to reduce the data dimensions of redundant feature parameters which come from decomposed IMFs by 2D-VMD algorithm and (2) the developed novel automated method is applied to screen normal and COVID-19 images, which shows pleasing diagnostic effect.

The rest of this article is organized as follows. The image dataset preprocessing and 2D-VMD method are given in Section 2. The main design for automated screening of COVID-19 (i.e., feature extraction, feature dimension reduction and classification) is presented in Section 3. The example verification and analysis results are given in Section 4. Finally, the conclusion is drawn in Section 5.

**Notation** The notation used throughout this paper is fairly standard.  $n$  represents the iteration number.  $\nabla$  is the second derivative.  $\tau$  denotes the time step.  $\|\cdot\|$  represents the Euclidean distance.  $\langle \cdot \rangle$  represents the dot product.  $\|\cdot\|_2$  is the 2-norm and  $\hat{u}$  is the Fourier transform.

## 2. Methodologies

### 2.1. Dataset acquisition and preprocessing

The COVID-19 medical radiography images were obtained from the COVID-19 dataset curated by Dr. Joseph Cohen [21]. The normal chest radiography medical images of pneumonia were obtained from the Kaggle dataset [22]. In this study, we have used 60 (30 normal and 30 COVID-19) images. Three normal and three COVID-19 images are shown in Figs. 1 and 2.

Image preprocessing plays an important role in obtaining an accurate classification result. First, in order to enhance the image contrast, the image dataset is processed by adaptive histogram homogenization [23]. At the same time, the bilinear interpolation algorithm is adopted to maintain uniformity. Then, the preprocessed images are resized to 48\*48 pixels.

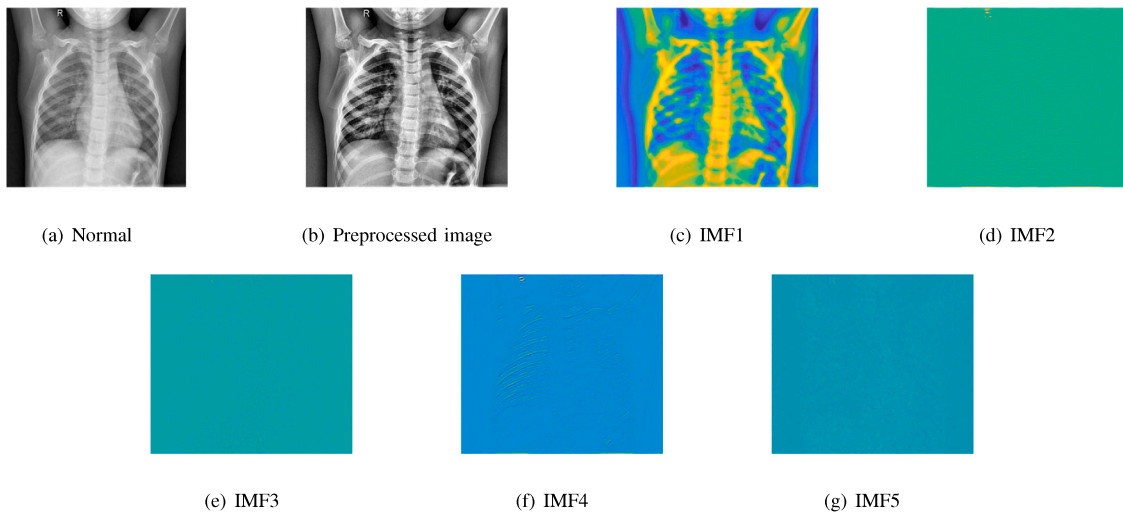


Fig. 3. The decomposed results of a normal image via 2D-VMD method.

## 2.2. The 2D-VMD method

The 2D-VMD method, as a non-recursive and adaptive decomposition method, is used to decompose images with minimal parameters. The 2D-VMD method is similar to VMD method in terms of the decomposition process [15,17,24]. The constrained variational equation is given by:

$$\min_{u_k, w_k} \left\{ \sum_k \alpha_k \left\| \nabla \left[ u_{AS,k}(x) e^{-j(w_k \cdot x)} \right] \right\|_2^2 \right\} \quad s.t. \quad \forall x : \sum_k u_k(x) = f(x) \quad (1)$$

where,  $u_{AS,k}(x)$  is mode.  $k = 1, \dots, K$  is the number of decomposed IMFs.  $w_k$  is central frequency of each IMF.  $f(x)$  is image signal and  $\alpha_k$  represents the penalty factor.

Eq. (1) can be expressed by using quadratic penalty factor and Lagrange multiplier. Then, it can be rewritten as follows:

$$L(\{u_k\}, \{w_k\}, \lambda) := \sum_k \alpha_k \left\| \nabla \left[ u_{AS,k}(x) e^{-j(w_k \cdot x)} \right] \right\|_2^2 + \left\| f(x) - \sum_k u_k(x) \right\|_2^2 + \left\langle \lambda(x), f(x) - \sum_k u_k(x) \right\rangle \quad (2)$$

where,  $\lambda$  is the Lagrange multiplier and  $\alpha$  is the quadratic penalty factor.

Further,  $u_k^{n+1}$ ,  $w_k^{n+1}$  and  $\lambda_k^{n+1}$  are updated until the termination condition has met  $\sum_k \left\| \hat{u}_k^{n+1} - \hat{u}_k^n \right\|_2^2 / \left\| \hat{u}_k^n \right\|_2^2 < K\epsilon$ . The specific decomposition process was given in [15].

The 2D-VMD algorithm requires assigning values to certain parameters, for example, decomposition scale  $K$  and penalty factor  $\alpha_k$  set in this work to 5 and 5000 respectively based on previous studies [16,20]. The decomposed IMFs of normal and COVID-19 radiography medical images by 2D-VMD method exhibit different texture patterns as shown in Figs. 3 and 4, respectively.

## 3. Feature optimization and selection

In this section, an automated method is presented to help imaging physicians to screen massive images for presence of COVID-19. Gabor filter is used to extract features of decomposed IMFs by 2D-VMD algorithm, and then a dimension reduction algorithm based on LLE is used in this paper when dimension reduction effect of which is compared with PCA. Subsequently, the parameters of SVM are optimized via PSO. Finally, the sensitive feature parameters are used as input into SVM for model training.

## 3.1. The feature extraction based on Gabor filter

In digital image processing, Gabor filter is a common feature extraction method. The expression of frequency and direction of Gabor filter is similar to that of the human visual system, also, it possesses good advantages in image texture representation. Therefore, up to now, Gabor wavelet has a good track record of application in the pattern recognition field [25–27]. In space domain, the expression of two-dimensional Gabor wavelet is described as follows:

Plural form:

$$g(x, y, \lambda, \theta, \psi, \sigma, \gamma) = \exp\left(-\frac{x'^2 + \gamma^2 y'^2}{2\sigma^2}\right) \exp\left(i\left(2\pi \frac{x'}{\lambda} + \psi\right)\right) \quad (3)$$

Real component:

$$g(x, y, \lambda, \theta, \psi, \sigma, \gamma) = \exp\left(-\frac{x'^2 + \gamma^2 y'^2}{2\sigma^2}\right) \cos\left(2\pi \frac{x'}{\lambda} + \psi\right) \quad (4)$$

Imaginary part:

$$g(x, y, \lambda, \theta, \psi, \sigma, \gamma) = \exp\left(-\frac{x'^2 + \gamma^2 y'^2}{2\sigma^2}\right) \sin\left(2\pi \frac{x'}{\lambda} + \psi\right) \quad (5)$$

where,  $x' = x \cos \theta + y \sin \theta$  and  $y' = -x \sin \theta + y \cos \theta$ .  $\lambda$  represents the wavelength of the sine function.  $\theta$  is the direction of the kernel function.  $\psi$  is the phase shift.  $\sigma$  is the Gaussian standard deviation.  $\gamma$  is the ellipticity of the Gabor function.  $x$  and  $y$  represent the coordinate positions of the pixel.

Typically, Gabor filter with different wavelengths and different directions is used to extract image features. In this article, Gabor filter has been selected with 5 scales and 8 directions. When an image passes through Gabor filter, it can be divided into  $5 \times 8 = 40$  sub-images with different scales and directions. Simultaneously, the bilinear interpolation is used to carry out down-sampling operation. Hence, extraction of an image by Gabor filters results in  $5 \times 8 \times 36 = 1440$  features. Here, decomposed IMF1 of a normal and a COVID-19 radiography medical images in Figs. 3 and 4 with Gabor filter resulted in  $5 \times 8 = 40$  sub-images with different scales and orientations respectively as shown in Fig. 5.

Extraction of image features via Gabor filter results in high dimensionality, and a large number of redundant feature parameters with same or similar performance which could affect the accuracy of the COVID-19 diagnosis. As such, it is necessary to reduce the dimensions of extracted features to extract low-dimensional parameters useful for COVID-19 diagnosis. Here, this task would be achieved by application of LLE algorithm.

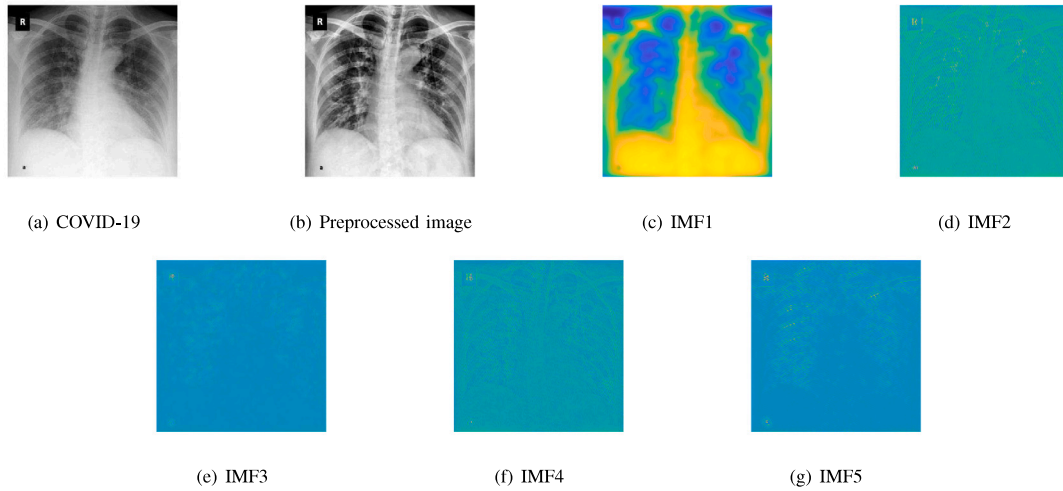


Fig. 4. The decomposed results of a COVID-19 image via 2D-VMD method.

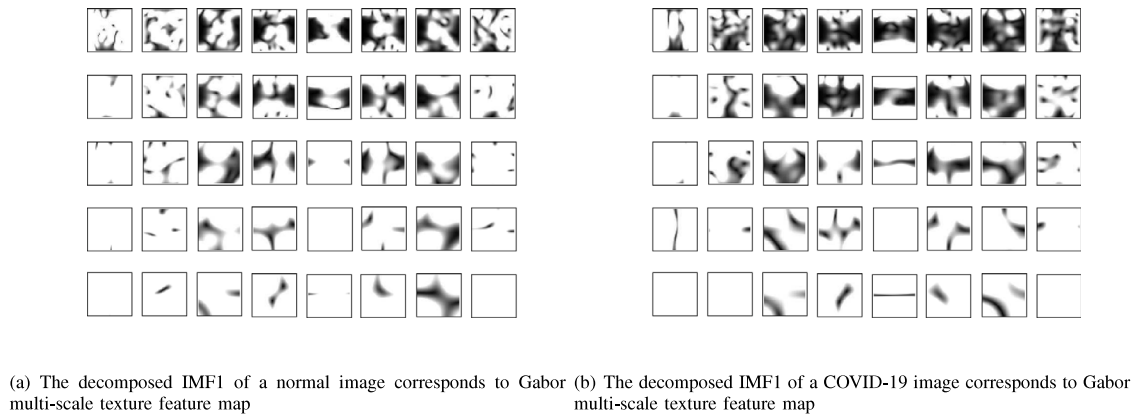


Fig. 5. The image processing effect via Gabor filter.

### 3.2. The feature optimization based on LLE algorithm

LLE algorithm, published in 2000 [28], is a nonlinear dimension reduction method based on manifold learning. The dimension reduction principle of LLE algorithm is to map the high-dimensional data to the low-dimensional space and to keep the original topology structure of the data after the dimension reduction. It not only has the advantages of a linear method but also has characteristics of a nonlinear algorithm [29,30]. The specific calculation process of LLE algorithm is described as follows:

Assume that the input data of LLE is  $X = [x_1, x_2, \dots, x_N]$ , in which  $x_i \in R^D$ . The obtained output data of dimension reduction via the LLE algorithm is  $Y = [y_1, y_2, \dots, y_N]$ ,  $y_i \in R^d$  and  $d \ll D$ .

(1) Selection of adjacent points: the Euclidean distance between each sample point  $X_i (i = 1, 2, \dots, N)$  and other  $N - 1$  sample points is calculated as follows:

$$d_{ij} = \left[ \sum_{k=1}^D |x_{ik} - x_{jk}|^p \right]^{\frac{1}{p}} \quad (6)$$

where,  $d_{ij}$  is the distance between the sample  $x_i$  and the sample  $x_j$ . If and only if  $p = 2$ ,  $d_{ij}$  represents the Euclidean distance between two points.

(2) Calculation of local reconstruction weight matrix  $W$ : the error function can be expressed as:

$$\epsilon(W) = \sum_{i=1}^N \left\| x_i - \sum_{j=1}^k w_{ij} x_{ij} \right\|_2^2 \quad (7)$$

where,  $x_{ij} (j = 1, 2, \dots, k)$  is the  $k$ th adjacent point of  $x_i$ ,  $w_{ij}$  represents the weight coefficient between the sample point  $x_i$  and its adjacent point  $x_{ij}$ . Under the condition of Formula (7) with  $\sum_{j=1}^k w_{ij} = 1$ .

When the value of error function is smaller, the reconstruction of local weight matrix is better. Also, when the error function is expressed as a matrix, the  $W$  can be obtained by using Lagrange multiplier method.

(3) Mapping of low-dimensional space: the  $d$ -dimensional embedding  $Y = [y_1, y_2, \dots, y_N]$ ,  $y_i \in R^d$  can be calculated by applying the weight matrix  $W$ .  $Y$  should satisfy the following conditions:

$$\min \phi(Y) = \sum_{i=1}^N \left\| y_i - \sum_{j=1}^k w_{ij} y_{ij} \right\|_2^2 \quad (8)$$

where,  $\phi(Y)$  is the loss function.  $y_{ij} (j = 1, 2, \dots, k)$  is the  $k$  adjacent points of  $y_i$ . Simultaneously, it satisfies the following two conditions:

$$\sum_{i=1}^N y_i = 0 \quad (9)$$

$$\frac{1}{N} \sum_{i=1}^N y_i y_i^T = I \quad (10)$$

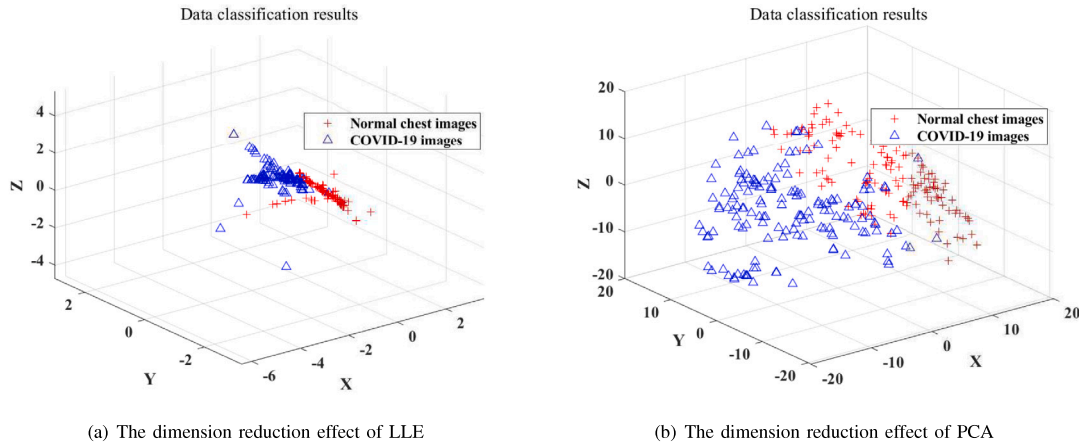


Fig. 6. The results of dimension reduction via LLE and PCA.

where,  $I$  represents the identity matrix.

Lagrange multiplier method is used to minimize loss function, from which it can be obtained  $MY^T = -\lambda Y^T$ . Here, the eigenvectors corresponding to the minimum  $d$  eigenvalues of matrix  $M$  are taken as the low-dimensional embedding result  $Y$ .

One example of experimental verification is shown to illustrate the dimension reduction effect of LLE and PCA. The starting number of normal and COVID-19 images is 30 each. Subsequently, features of the decomposed IMFs are extracted by Gabor filter, and then high-dimension features are reduced by LLE and PCA to get informative features. The results of dimension reduction are shown in Fig. 6, where red '+' represents normal and blue 'Δ' represents COVID-19. It can be seen that LLE clusters same type images quite well resulting in almost complete separation of two different type images, thus signifying the diagnostic value of this approach. On the other hand, PCA results in a more interspersed pattern where the two types of image data could not be separated well. Therefore, in this paper, LLE algorithm is utilized to reduce the dimensions of redundant features parameters.

### 3.3. SVM classifier

SVM is a machine learning method that works well with small sample numbers and in cases when nonlinear pattern recognition is required, and therefore is widely used in classification algorithms [31, 32]. The SVM algorithm maps nonlinear transformation to a high-dimensional space via kernel function, where it constructs linear discriminant function and seeks to establish an optimal classification hyper plane. Based on the above-mentioned procedures, it has an ability to solve the nonlinear problem. In this paper, the SVM model is based on the following Radial Basis Function (RBF) kernel:

$$K(x_i, x_j) = e^{-\frac{\|x_i - x_j\|^2}{2\sigma^2}} \quad (11)$$

where,  $(x_i, x_j)$  is data sample,  $\sigma$  is used to dominate radial range of function.

In SVM classification process, it is difficult for one evaluation method to correctly evaluate classification effect. In general, a combination of multiple evaluation indicators is used to evaluate classification effect of an SVM classifier. In this paper, different evaluation indicators e.g., accuracy, precision, recall and F-Measure, are used to evaluate the performance of the classification model. Confusion matrix is a common indicator to evaluate the effectiveness of algorithms and includes true positive (TP), false positive (FP), true negative (TN) and false negative (FN).

$$\text{Accuracy} = \frac{TP + TN}{TP + TN + FP + FN} \quad (12)$$

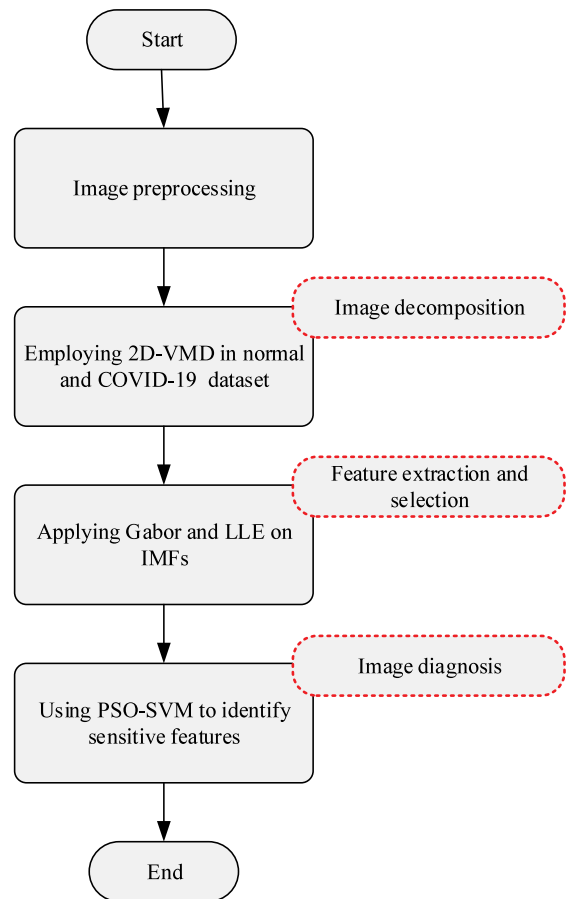


Fig. 7. The flowchart of the COVID-19 diagnosis technology.

Accuracy is the most common index in a classification model, and it can directly give the accuracy of a classification model. The value range of accuracy is [0, 1], and perfect classification equals 1.

$$\text{Precision} = \frac{TP}{TP + FP} \quad (13)$$

The value range of precision is [0, 1], and perfect classification equals 1.

$$\text{Recall} = \frac{TP}{TP + FN} \quad (14)$$

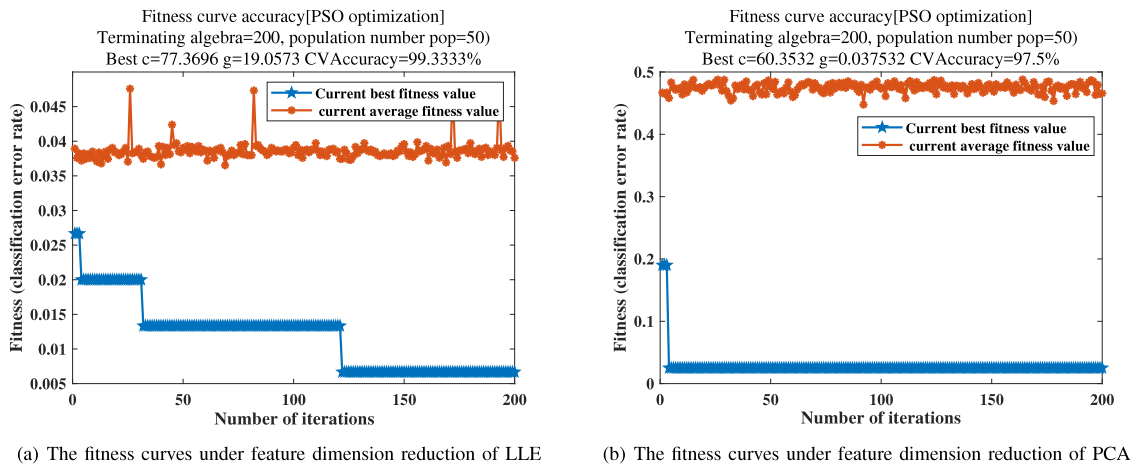


Fig. 8. The particle swarm fitness curves.

The recall represents the proportion of identified positive cases among all actual positive cases.

$$F - \text{Measure} = 2 \cdot \frac{\text{Pr } precision \cdot \text{Recall}}{\text{Pr } precision + \text{Recall}} \quad (15)$$

The main function of F-Measure is to balance accuracy and recall.

### 3.4. PSO parameter optimization

PSO algorithm is an optimization algorithm based on swarm intelligence. Also, it utilizes iterative method to find the optimal solution. In the optimization process, PSO algorithm mainly involves three variables, i.e., speed, position and fitness function. Both individual optimization and global optimization are applied via the particle to continuously update its speed and position in each iteration process [33, 34].

Suppose that there is a  $D$ -dimensional search space in which  $N$  particles constitute a population. In the search space, the position and the flight speed of  $i$ th particle are represented by  $X_i = (x_{i1}, x_{i2}, \dots, x_{iD})$  and  $V_i = (v_{i1}, v_{i2}, \dots, v_{iD})$ , respectively. The current optimal search position of  $i$ th particle and entire population can be represented by  $p_i = (p_{i1}, p_{i2}, \dots, p_{iD})$  and  $p_g = (p_{g1}, p_{g2}, \dots, p_{gD})$ , respectively. In the process of optimization, particles update position and velocity according to the following two formulas:

$$v_{id}^{l+1} = w * v_{id}^l + c_1 * r_1 * (p_{id}^l - x_{id}^l) + c_2 * r_2 * (p_{gd}^l - x_{id}^l) \quad (16)$$

$$x_{id}^{l+1} = v_{id}^{l+1} + x_{id}^l \quad (17)$$

where,  $w$  is the weight of inertia.  $c_1$  and  $c_2$  are the learning factors.  $r_1$  and  $r_2$  are the random numbers in  $[0, 1]$ .  $l$  is the current number of iterations.  $x_{id}^l$  is the  $d$ -dimensional position of  $i$ th particle in the  $l$ th iteration.  $v_{id}^{l+1}$  is the  $d$ -dimensional velocity of  $i$ th particle in the  $(l+1)$ th iteration.

### 3.5. Combination of PSO and SVM

SVM algorithm has two very important parameters, i.e., penalty factor  $c$  and kernel parameter  $g$ , which can affect the accuracy of COVID-19 diagnosis. In this paper, PSO algorithm is adopted to optimize SVM to find the optimal parameters of  $c$  and  $g$ . Here, the accuracy of classification is used as fitness function. Initially, the position and velocity of the particle swarm need to be initialized. Then, both the optimum of the individual particle and the global optimum of the population are calculated. Finally, the velocity and position of the particle are constantly updated until the stop condition is satisfied, from which we can obtain the optimal parameters of  $c$  and  $g$  [35].

**Table 1**  
Parameters used in PSO.

Parameters of PSO	Values
$c_1$	1.5
$c_2$	1.7
Maximum population	20
Maximum number of evolution	200

Next, the flowchart of the COVID-19 diagnosis method in the paper is shown in Fig. 7, the specific steps are as follows:

- (1) the normal and COVID-19 datasets are decomposed by the 2D-VMD algorithm, and several IMFs are obtained.
- (2) based on a combination of Gabor and LLE, feature extraction and selection of decomposed IMFs are performed.
- (3) sensitive features are identified by the combination of PSO and SVM for the COVID-19 diagnosis.

## 4. Example verification and analysis

In this section, the normal and COVID-19 images are applied to verify validity of the designed diagnosis technology. Subsequently, in view of practical application that the graphical user interface (GUI) in Matlab software is used to design a more intuitive COVID-19 image diagnosis system interface, which can directly present the diagnosis results to facilitate diagnosis and treatment for imaging physicians.

### 4.1. Example verification

For used normal and COVID-19 images, each image is decomposed by 2D-VMD to five IMFs, and as a result, both the number of normal and COVID-19 images are extended to  $5 \times 30 = 150$ , respectively. The image features are extracted by Gabor filter resulting in  $5 \times 8 \times 36 = 1440$  features per image. The redundant features are diminished by LLE algorithm, followed by classification using SVM classifier with RBF kernel. In the experiment, PSO is used to optimize SVM to find the optimal parameters of  $c$  and  $g$ . Initial parameters for PSO are set as follows (see Table 1).

The experiment has randomly utilized 150 samples for training and the remaining 150 samples for testing. The particle swarm fitness curves are plotted in Fig. 8. From Fig. 8, it can be clearly seen that  $c = 77.3696$  and  $g = 19.0573$  under the feature dimension reduction via LLE, also,  $c = 60.3532$  and  $g = 0.037532$  under the feature dimension reduction via PCA.

The parameters obtained by PSO optimization have been used to establish the SVM classification models (LLE-PSO-SVM model and PCA-PSO-SVM model), and the classification results are shown in Fig. 9.

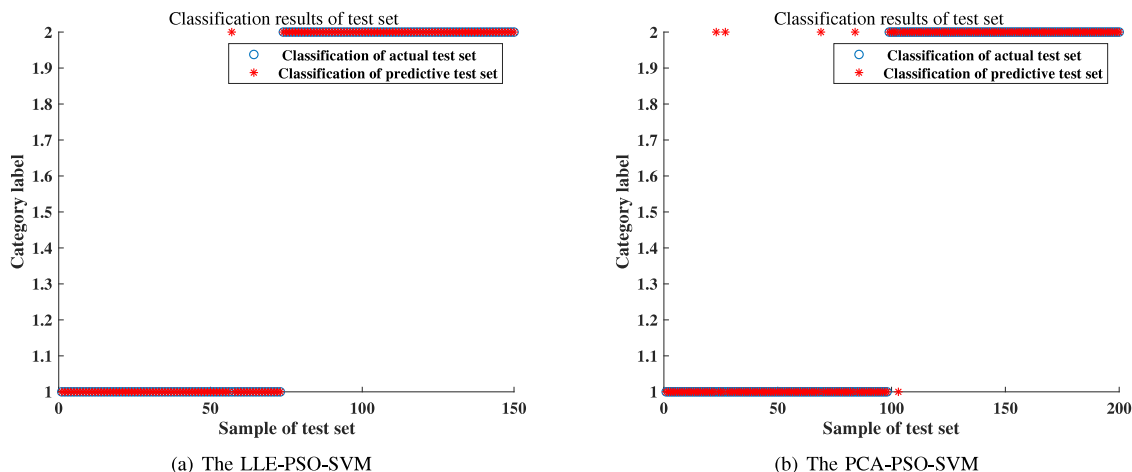


Fig. 9. The recognition effects based on the LLE-PSO-SVM model and the PCA-PSO-SVM model.

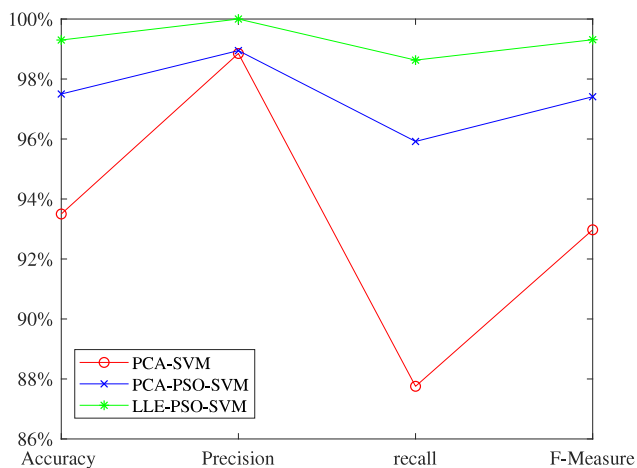


Fig. 10. The performance measures of three methods.

Fig. 9 clearly shows that the LLE-PSO-SVM model has better recognition effect compared with the PCA-PSO-SVM model.

To verify the effectiveness of the proposed automated method for screening of normal and COVID-19 images, the different evaluation indicators e.g., accuracy, precision, recall and F-Measure, are used to evaluate performance of diagnosis methods. Fig. 10 shows the performance measures of three methods, from which, it can be seen that the proposed diagnosis method has the satisfactory performance compared with the other two methods. The proposed method has achieved accuracy of 99.33%, precision of 100%, recall of 98.63% and F-Measure of 99.31%.

Additionally, to further illustrate the validity of the proposed novel method, we vary the number of samples. Here, we increase the amount of data, by using 90 normal and 90 COVID-19 images. Each image will be decomposed by 2D-VMD method to five IMFs, and as a result, both the number of normal and the number of COVID-19 images can be extended to  $5 \times 90 = 450$ , respectively. Similarly, the different evaluation indicators (i.e., accuracy, precision, recall and F-Measure) are used to evaluate the performance of the developed diagnosis method. The performance measures of three methods are shown in Fig. 11.

As can be seen in Fig. 11, LLE-PSO-SVM method has consistently better diagnosis performance compared with PCA-SVM method and

PCA-PSO-SVM method based on better values of the evaluation indicators. Across different numbers of samples, thus further confirming the effectiveness of the novel diagnosis technology proposed in this paper.

#### 4.2. GUI design

The GUI is presented based on the design diagnosis method so that imaging physicians can repeat the analysis and use the interface in their day-to-day multi-block data analysis tasks. There are image pre-processing, image feature extraction, image diagnostic model building and verification in interface. The diagnosis interface is shown in Fig. 12.

The image data obtained from Dr. Joseph Cohen and Kaggle dataset is used to establish diagnostic model. After image preprocessing, the data is ready for multi-block image analysis. Once the image data is loaded, the figure will be updated in the GUI. When the COVID-19 image diagnostic model has established in interface, an example is used to verify the effectiveness of the established diagnostics model.

We use clinical images to test the designed diagnostic system of COVID-19 image. When a COVID-19 image is input to the established diagnostic model, subsequently, GUI outputs “This image is a COVID-19 image!”. The interface of image diagnosis result is shown in Fig. 13.

We have randomly used 20 images (17 normal and 3 COVID-19) to test, and then the predicted result is in good agreement with the actual type. Also, the designed GUI can perform well and all the options are fully functional. It is noteworthy that there is a main advantage based on COVID-19 image diagnostic system of GUI, namely, it can be easily used to facilitate diagnosis and treatment for imaging physicians, and therefore it makes practical sense to research into the issue based on COVID-19 image diagnostic system of GUI.

#### 5. Conclusions

In this article, we have proposed a novel computer aided diagnosis for automatic processing of normal and COVID-19 images. The effectiveness of the proposed method has been validated on specific examples. From the obtained results, we can conclude that a combination of 2D-VMD algorithm and LLE algorithm is useful to get informative features which are beneficial for classification. On the other hand, it has been concluded that the proposed diagnosis method has achieved satisfactory performance characteristics, and it could therefore be useful in COVID-19 diagnostics. In future, we intend to develop a CAD tool for other diseases (e.g., glaucoma diagnosis [36], multi-class brain abnormalities [18] and congenital heart disease [20]). Also, we intend to improve the diagnosis performance using deep learning method.

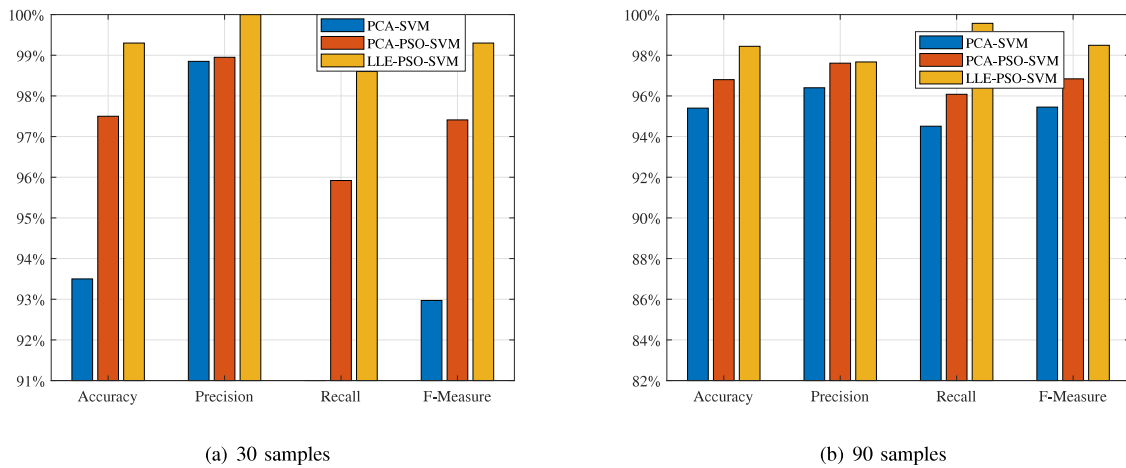


Fig. 11. The performance measures of three methods based on different samples.

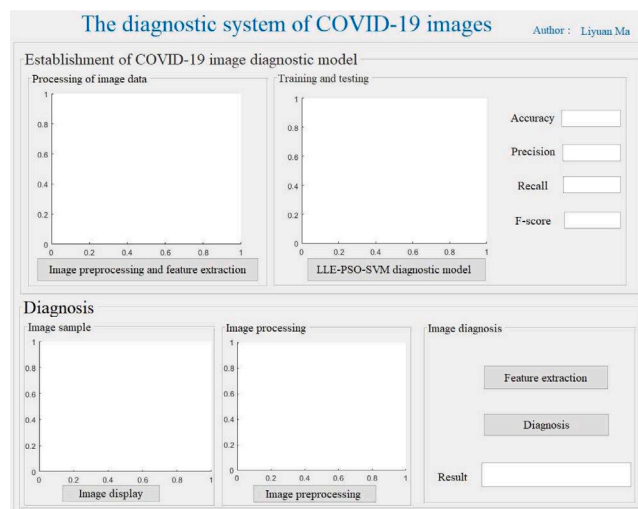


Fig. 12. The interface of COVID-19 image diagnostic system.

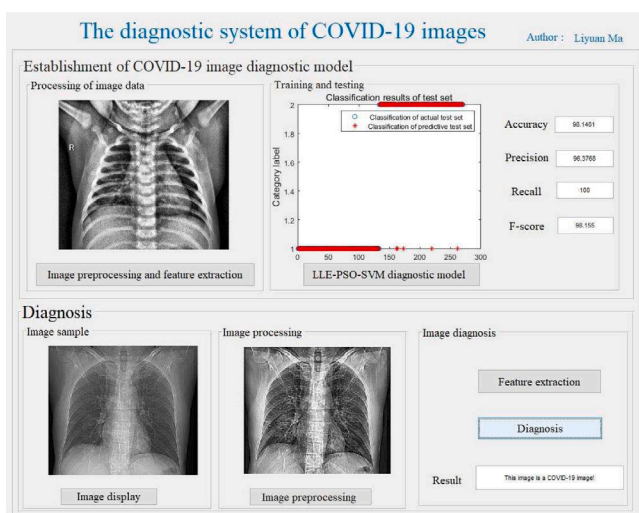


Fig. 13. The interface of image diagnosis result.

### Funding

Introductory Project of Fujian Provincial Science and Technology Plan, China (2020Y01010048), Science and Technology Program of Ningbo City (2019A610234), Medical and Health Program of Zhejiang Province (2020KY854).

### CRediT authorship contribution statement

**Liyuan Ma:** Conceptualization, Methodology, Software, Writing – original draft. **Xipeng Xu:** Supervision. **Changcai Cui:** Validation, Formal analysis, Writing – review & editing. **Jingyi Lu:** Formal analysis, Writing – review & editing. **Qifeng Hua:** Funding acquisition. **Hao Sun:** Funding acquisition.

### Declaration of competing interest

No author associated with this paper has disclosed any potential or pertinent conflicts which may be perceived to have impending conflict with this work. For full disclosure statements refer to <https://doi.org/10.1016/j.bspc.2022.103889>.

### Acknowledgments

The authors would like to thank Dr. Joseph Cohen at University of Montreal for sharing the X-ray images of COVID-19 patients publicly

and would like to thank Kaggle repository for sharing normal chest radiography medical images of pneumonia, which helped significantly to make this work possible. The authors would also like to acknowledge Dr. Prof. Philipp Kapranov of the Institute of Genomics, School of Medicine of Huaqiao University for providing detailed modifications for this paper.

## References

- [1] L. Duran-Lopez, J.P. Dominguez-Morales, J. Corral-Jaime, COVID-XNet: A custom deep learning system to diagnose and locate COVID-19 in chest x-ray images, *Appl. Ences* 10 (16) (2020) 5683–5694, <http://dx.doi.org/10.3390/app10165683>.
- [2] N. Poyiadji, G. Shahin, D. Noujaim, COVID-19 associated acute hemorrhagic necrotizing encephalopathy: imaging features, *Radiology* 296 (2) (2020) 119–120, <http://dx.doi.org/10.1148/radiol.2020201187>.
- [3] W. Wang, J. Tang, F. Wei, Updated understanding of the outbreak of 2019 novel coronavirus (2019-nCoV) in Wuhan, China, *Wiley-Blackwell Online Open* 92 (4) (2020) 441–447, <http://dx.doi.org/10.1002/jmv.25689>.
- [4] Z. Zu, M. Jiang, P. Xu, Coronavirus disease 2019 (COVID-19): A perspective from China, *Radiology* 296 (2) (2020) 15–25, <http://dx.doi.org/10.1148/radiol.2020200490>.
- [5] I.L. Giacomelli, R. Schuhmacher Neto, E. Marchiori, Chest x-ray and chest ct findings in patients diagnosed with pulmonary tuberculosis following solid organ transplantation: A systematic review, *Jornal Brasileiro de Pneumologia* 44 (2) (2018) 161–166, <http://dx.doi.org/10.1590/S1806-37562017000000459>.
- [6] E.A. El-Dahshan, A.B.M. Salem, T.H. Younis, A hybrid technique for automatic MRI brain images classification, *Studia Univ. Babeş-Bolyai : Ser. Inform.* 54 (1) (2009) 55–67.
- [7] S. Chaplot, L.M. Patnaik, N.R. Jagannathan, Classification of magnetic resonance brain images using wavelets as input to support vector machine and neural network, *Biomed. Signal Process. Control* 1 (1) (2006) 86–92, <http://dx.doi.org/10.1016/j.bspc.2006.05.002>.
- [8] Y. Peng, Y. Tang, S. Lee, COVID-19-CT-CXR: A freely accessible and weakly labeled chest X-ray and CT image collection on COVID-19 from biomedical literature, *IEEE Trans. Big Data* 7 (1) (2021) 3–12, <http://dx.doi.org/10.1109/TBDATA.2020.3035935>.
- [9] J.A. Baker, E.L. Rosen, J.Y. Lo, Computer-aided detection (CAD) in screening mammography: sensitivity of commercial CAD systems for detecting architectural distortion, *Ajr Am. J. Roentgenol.* 181 (4) (2003) 1083–1088, <http://dx.doi.org/10.2214/ajr.181.4.1811083>.
- [10] R. Harikumar, B. Vinoth kumar, Performance analysis of neural networks for classification of medical images with wavelets as a feature extractor, *Int. J. Imaging Syst. Technol.* 25 (1) (2015) 33–40, <http://dx.doi.org/10.1002/ima.22118>.
- [11] Y. Zhang, Z. Dong, A. Liu, Magnetic resonance brain image classification via stationary wavelet transform and generalized eigenvalue proximal support vector machine, *J. Med. Imaging Health Inform.* 5 (7) (2015) 1395–1403, <http://dx.doi.org/10.1166/jmihi.2015.1542>.
- [12] Z. Masetic, A. Subasi, Congestive heart failure detection using random forest classifier, *Comput. Methods Programs Biomed.* 130 (2016) 54–64, <http://dx.doi.org/10.1016/j.cmpb.2016.03.020>.
- [13] H. Kalbkhani, M.G. Shayesteh, B. Zali-Vargahan, Robust algorithm for brain magnetic resonance image (mri) classification based on garch variances series, *Biomed. Signal Process. Control* 8 (6) (2013) 909–919, <http://dx.doi.org/10.1016/j.bspc.2013.09.001>.
- [14] V. Ravi, H. Narasimhan, T.D. Pham, A cost-sensitive deep learning-based meta-classifier for pediatric pneumonia classification using chest X-rays, *Expert Syst.* (2020) <http://dx.doi.org/10.1111/exsy.12966>.
- [15] K. Dragomiretskiy, D. Zosso, *Two-Dimensional Variational Mode Decomposition*, Vol. 8932, Springer International Publishing, 2015, pp. 197–208, [http://dx.doi.org/10.1007/978-3-319-14612-6\\_15](http://dx.doi.org/10.1007/978-3-319-14612-6_15).
- [16] H. Gao, L. Ma, H. Dong, An improved two-dimensional variational mode decomposition algorithm and its application in oil pipeline image, *Syst. Sci. Control Eng.* 8 (1) (2020) 297–307, <http://dx.doi.org/10.1080/21642583.2020.1756523>.
- [17] K. Dragomiretskiy, D. Zosso, Variational mode decomposition, *IEEE Trans. Signal Process.* 62 (3) (2013) 531–544, <http://dx.doi.org/10.1109/TSP.2013.2288675>.
- [18] A. Gudigar, U. Raghavendra, E.J. Ciaccio, Automated categorization of multi-class brain abnormalities using decomposition techniques with MRI images: A comparative study, *IEEE Access* 7 (2019) 28498–28509, <http://dx.doi.org/10.1109/ACCESS.2019.2901055>.
- [19] S. Maheshwari, R.B. Pachori, V. Kanhangad, Iterative variational mode decomposition based automated detection of glaucoma using fundus images, *Comput. Biol. Med.* 88 (2017) 142–149, <http://dx.doi.org/10.1016/j.compbiomed.2017.06.017>.
- [20] U. Raghavendra, U.R. Acharya, A. Gudigar, Automated screening of congestive heart failure using variational mode decomposition and texture features extracted from ultrasound images, *Neural Comput. Appl.* 28 (2017) 2869–2878, <http://dx.doi.org/10.1007/s00521-017-2839-5>.
- [21] J.P. Cohen, P. Morrison, L. Dao, Covid-19 image data collection: Prospective predictions are the future, *J. Mach. Learn. Biomed. Imaging* 1 (2020) 1–38, <http://dx.doi.org/10.48550/arXiv.2006.11988>.
- [22] [www.kaggle.com](http://www.kaggle.com), Retrieved March 27, 2020.
- [23] J. Mrquez, F. Schmitt, Radiometric homogenization of the color cryosection images from the VHP lungs for 3D segmentation of blood vessels, *Radiology* 24 (3) (2000) 181–191, [http://dx.doi.org/10.1016/S0895-6111\(00\)00018-5](http://dx.doi.org/10.1016/S0895-6111(00)00018-5).
- [24] J. Lu, J. Yue, L. Zhu, Variational mode decomposition denoising combined with improved Bhattacharyya distance, *Measurement* 151 (2020) <http://dx.doi.org/10.1016/j.measurement.2019.107283>.
- [25] D.A. Clausi, H. Deng, Design-based texture feature fusion using gabor filters and co-occurrence probabilities, *IEEE Trans. Image Process.* 14 (7) (2005) 925–936, <http://dx.doi.org/10.1109/TIP.2005.849319>.
- [26] C. Liu, Gabor-based kernel PCA with fractional power polynomial models for face recognition, *IEEE Trans. Pattern Anal. Mach. Intell.* 26 (5) (2004) 572–581, <http://dx.doi.org/10.1109/TPAMI.2004.1273927>.
- [27] B. Kubicek, A.S. Gupta, I. Kirsteins, Sonar target representation using two-dimensional gabor wavelet features, *J. Acoust. Soc. Am.* 148 (4) (2020) 2061–2072, <http://dx.doi.org/10.1121/10.0002168>.
- [28] S.T. Roweis, L.K. Saul, Nonlinear dimensionality reduction by locally linear embedding, *Science* 290 (5500) (2000) 2323–2326, <http://dx.doi.org/10.1126/science.290.5500.2323>.
- [29] L.K. Saul, S.T. Roweis, Think globally, fit locally: unsupervised learning of low dimensional manifolds, *J. Mach. Learn. Res.* 4 (2) (2003) 119–155, <http://dx.doi.org/10.1162/153244304322972667>.
- [30] J. Vanderplas, A. Connolly, Reducing the dimensionality of data: locally linear embedding of sloan galaxy spectra, *Astron. J.* 138 (5) (2009) 1365–1379, <http://dx.doi.org/10.1088/0004-6256/138/5/1365>.
- [31] C. Cortes, V.N. Vapnik, Support-vector networks, *Mach. Learn.* 20 (3) (1995) 273–297, <http://dx.doi.org/10.1007/BF00994018>.
- [32] S.L. Salzberg, On comparing classifiers: pitfalls to avoid and a recommended approach, *Data Min. Knowl. Discov.* 1 (3) (1997) 317–328, <http://dx.doi.org/10.1023/A:1009752403260>.
- [33] R. Poli, J. Kennedy, T. Blackwell, Particle swarm optimization, *J. Acoust. Soc. Am.* 1 (1) (2007) 33–57, <http://dx.doi.org/10.1007/s11721-007-0002-0>.
- [34] G. Venter, J. Sobieszczanski-Sobieski, Particle swarm optimization, *AIAA J.* 41 (8) (2003) 1583–1589, <http://dx.doi.org/10.2514/2.2111>.
- [35] Y. Ren, G. Bai, Determination of optimal SVM parameters by using GA/PSO, *J. Comput. Phys.* 5 (8) (2010) 1160–1168, <http://dx.doi.org/10.4304/jcp.5.8.1160-1168>.
- [36] K. Chan, T.W. Lee, P.A. Sample, Comparison of machine learning and traditional classifiers in glaucoma diagnosis, *IEEE Trans. Biomed. Eng.* 49 (9) (2002) 963–974, <http://dx.doi.org/10.1109/TBME.2002.802012>.